metals

MDPI

Article

Effect of Thermo-Mechanically Activated Precipitation on the Hot Deformation Behavior of High Strength Aluminum Alloy AA7075

Emad Scharifi [1,*], Jürgen A. Nietsch [2], Angela Quadfasel [2], Ursula Weidig [1] and Kurt Steinhoff [1]

[1] Metal Forming Technology, University of Kassel, Kurt-Wolters-Straße 3, 34125 Kassel, Germany
[2] Institute of Metal Forming (IBF), RWTH Aachen University, 52072 Aachen, Germany
* Correspondence: emad.scharifi@uni-kassel.de; Tel.: +49-561-804-1973

Abstract: The present study investigates the effect of two different microstructural conditions on the hot deformation behavior of precipitation-hardenable AA7075 by compression tests ranging from 200 °C to 350 °C and strain rates from 0.1 s^{-1} to 10 s^{-1}. The first condition is solution heat-treated and quenched in water, whereas the second condition is achieved by subsequent artificial aging and stabilization for 24 h at the respective intended deformation temperature. Both conditions indicate an increase in flow stress with increasing strain rate and decreasing deformation temperature. Moreover, with increasing deformation temperature and decreasing strain rate, the flow behavior gradually changes as dynamic recrystallization becomes the dominant factor for the flow curve appearance. At the same deformation temperature, higher flow stresses are obtained for the as-quenched condition due to the dynamic precipitation and growth of very small precipitates (r < 20 nm) during hot deformation. For the deformation temperature of 200 °C and the strain rate of 10 s^{-1}, higher peak stresses of 110 MPa are obtained for the as-quenched condition. This is confirmed by the transmission electron microscopy investigations, which show the formation of very fine precipitates for the as-quenched condition, while coarse precipitates can be found in the stabilized microstructure. Despite this observation, the work hardening analysis reveals lower strain-hardening rates for the as-quenched condition and higher critical stresses for the onset of dynamic recrystallization compared to the thermally stabilized microstructure.

Keywords: hot deformation; dynamic precipitation; thermo-mechanical softening mechanisms

Citation: Scharifi, E.; Nietsch, J.A.; Quadfasel, A.; Weidig, U.; Steinhoff, K. Effect of Thermo-Mechanically Activated Precipitation on the Hot Deformation Behavior of High Strength Aluminum Alloy AA7075. *Metals* **2022**, *12*, 1609. https://doi.org/10.3390/met12101609

Academic Editors: Maciej Motyka, Mats Oldenburg and Jens Hardell

Received: 16 August 2022
Accepted: 21 September 2022
Published: 26 September 2022

1. Introduction

Dynamic recovery, dynamic recrystallization and thermally activated precipitation are competitive, sometimes simultaneously appearing mechanisms governing the microstructure evolution and the flow behavior of precipitation-hardenable aluminum alloys during hot forming operations. Whilst dynamic recovery and dynamic recrystallization are typical softening mechanisms during hot deformation of precipitation-hardenable aluminum alloys, leading to a decrease in flow stress [1,2], thermally activated precipitation is known as a strengthening mechanism resulting in an increase in flow stress [3,4]. The driving force for the occurrence of these mechanisms is the stored energy in the crystal structure caused by straining or plastic deformation resulting in a high dislocation density, which can be removed again by recrystallization. In this regard, Steinhoff et al. indicate that a partial recrystallization can preserve high dislocation density and stored mechanical energy by proposing a novel modified process chain [5,6]. During the recrystallization process, it is reported that the dislocation density is reduced to an equilibrium value of $10^{10}/m^2$ [7]. It is further shown that a remaining density dislocation of $1.5 \times 10^{14}/m^2$, is high enough to drive the softening process such as recrystallization [8]. Accordingly, for the precipitation aluminum alloy AA2195, it is shown that at temperatures between 300 °C and 360 °C, discontinuous dynamic recrystallization is the main softening mechanism triggered

by prior plastic deformation and sufficient dislocation density. At higher temperatures between 420 °C and 520 °C, geometric dynamic recrystallization occurs involving three types of subgrain-forming mechanisms [9].

The high stacking fault energy of aluminum alloys favors the high rate of dynamic recovery caused by dislocation climb and cross-slip during plastic deformation [10]. At elevated deformation temperatures, consequently, the probability of cross-slip increases driven by the rise of lattice vibration and vacancy annihilation. On the microscopical level, dynamic recovery is based on the interaction of long-range stress fields between dislocations. This leads to organized dislocation structures and arrangements in the shape of low-angle grain boundaries, consequently reducing internal stresses. Dynamic recrystallization, in contrast, is based on the nucleation and growth of new grains and is characterized by the migration of high-angle boundaries and the elimination of a high number of dislocations [11–14].

Hence, at deformation temperatures above the recrystallization temperature, the accumulation of plastic strain and thermal activation continuously provokes the onset of dynamic recrystallization leading to a distinctive softening and drop in flow stress [15–17].

For a comprehensive understanding of the flow behavior during the hot forming of precipitation-hardenable aluminum alloys, the effect of solute atmosphere concentration and the underlying dynamical formation of clusters and precipitates, so-called dynamic precipitation, has to be taken into account. Dynamic precipitation is characterized by the homogenous formation of very fine precipitates during hot deformation, due to the increased defect density and nucleation sites [13,18,19]. This solid-state reaction plays a key role in the microstructural evolution and hence the flow behavior of precipitation-hardenable aluminum alloys during hot forming operations. Therefore, several studies have been conducted in the past to shed light on the principle of thermo-physical responses to nucleation and growth of precipitates. The focus of these investigations is on the severe plastic deformation processes, e.g., the equal channel angular extrusion process (ECAP), [20,21], the microstructural appearance of precipitates [20,22,23] and their contribution to the mechanical properties [24]. The increase in mechanical properties at room temperature is reported to be significantly affected by the interaction of dynamic precipitation and dynamic recrystallization [24]. It is concluded that the dynamic precipitates form before the onset of the dynamic recrystallization and consequently affect the dynamic recrystallization. Moreover, tensile experiments on precipitation-hardenable aluminum Al-Zn-Mg-Cu alloy revealed a size and intensity dependence of the precipitates on the strain rate [23]. As a consequence of this, deformation-enhanced precipitation processes are therefore able to significantly increase the flow stress and strain-hardening rate of the precipitation-hardenable aluminum alloy AA7075. For example, a significant hardening from 177 MPa (yield stress) to 331 MPa (tensile strength) is observed at a deformation temperature (DT) of $T_{DT} = 200$ °C and a strain rate of $\dot{\varepsilon} = 0.1$ s^{-1} [15], due to the accelerated formation of very fine precipitates and their interaction with mobile dislocations. Further investigations on Mg-9Al-1Zn and Mg-Al-Sn alloys reveal that the volume percentage of dynamically recrystallized grains is related to the amount of nucleated particles during hot deformation [25,26]. Therefore, for hot deformation of metastable conditions, such as a supersaturated solid solution or as-quenched condition, dynamic precipitation and its interaction with dynamic softening mechanisms constitutes a key phenomenon, in order to understand the hardening mechanisms and hot flow behavior at different temperatures and strain rates up to $\dot{\varepsilon} = 10$ s^{-1}.

Taking the above-presented studies into account, it is obvious that the microstructure condition, especially precipitate phases, and phase stability address open questions in the scope of the complex deformation behavior of precipitation-hardenable aluminum alloys at elevated temperatures. For that reason, the aim of the present study is to investigate the influence of different microstructural conditions and ultimately the influence of dynamic precipitation and dynamic softening at a wide range of strain rates from $\dot{\varepsilon} = 0.1$ s^{-1} up to $\dot{\varepsilon} = 10$ s^{-1} and deformation temperatures of $T_{DT} = 200$ °C up to $T_{DT} = 350$ °C on the hot

deformation behavior of the precipitation-hardenable aluminum alloy AA7075. Moreover, a detailed comparison of the effect of phase stability induced by different heat treatment strategies and the structural relation of precipitate phases on the strain-hardening behavior is presented.

2. Materials and Methods

2.1. Investigated Material

The experimental investigation is carried out on the precipitation-hardenable aluminum alloy AA7075 (Al-Zn-Mg(-Cu)) [27,28]. The material was received as extruded rod with a diameter of 14 mm in T6 condition (solution heat-treated, quenched in water and artificially aged). The chemical composition is given in Table 1. For the compression tests, cylindrical samples with a height of 18 mm and a diameter of 12 mm were machined from the as-received bars. The as-received microstructure can be found in [29].

Table 1. Chemical composition of the investigated precipitation-hardenable aluminum alloy AA7075.

Element	Si	Fe	Cu	Mn	Mg	Cr	Zn	Ti	Zr	Al
Mass content in %	0.10	0.11	1.49	0.03	2.38	0.20	5.57	0.03	0.04	Balance

2.2. Heat Treatment and Hot Deformation Experiments

The first group of experiments aims at the investigation of hot deformation behavior of the metastable as-quenched condition. For this purpose, the investigated material is solution heat-treated (SHT) at $T_{SHT} = 480$ °C for $t_{SHT} = 30$ min [30,31] to homogenize and dissolve the alloying elements into solid solution and rapidly quenched in water to obtain a high cooling rate. Immediately after the heat treatment, the as-quenched samples were deformed at different deformation temperatures (DT) ranging from $T_{DT} = 200$ °C to $T_{DT} = 350$ °C and strain rates of $\dot{\varepsilon} = 0.1\ s^{-1}$ to $\dot{\varepsilon} = 10\ s^{-1}$, as shown in Table 2.

Table 2. Main experimental parameters used in this work.

Material	T_{SHT} °C	T_{SHT} min	Artificial Aging (°C)/h	Deformation Temperature °C	Strain Rate s^{-1}
AA7075—As-quenched	480	30	-	200, 250, 300, 350	0.1, 1, 10
A7075—TSM	480	30	(200, 250, 300, 350)/24	200, 250, 300, 350	0.1, 1, 10

The second group of experiments aims at the investigation of hot deformation behavior of a thermally stabilized microstructure. Therefore, the investigated material is first solution heat-treated at $T_{SHT} = 480$ °C for $t_{SHT} = 30$ min and quenched in water. The compression test specimens were then artificially aged (AA) for $t_{AA} = 24$ h at the respective deformation temperature ranging from $T_{DT} = 200$ °C to $T_{DT} = 350$ °C, see Table 2. These samples are referred to as the thermally stabilized microstructure (TSM).

2.3. Property Characterization and Microstructure Investigation

All hot deformation experiments in the present study were conducted according to a flow curve determination guideline published by German industrial associations [32] using a servo-hydraulic press (thermo-mechanical treatment simulator from Servotest Testing Systems Ltd., Egham, UK) with a maximum compression force capacity of 1200 kN and a max. tool speed of 3000 mm/s. To avoid contact friction between tools and specimen surfaces during the experiments, Teflon foils were used for all temperatures and strain rates [33]. Due to the rise of sample temperature during plastic deformation by dissipated heat, the flow stresses were compensated, according to Kopp et al. [33]. Note that for each tested deformation temperature and strain rate, three repetitions were conducted.

The microstructure investigations of the specimens formed at $T_{DT} = 200$ °C and strain rates of $\dot{\varepsilon} = 0.1$ s^{-1} and $\dot{\varepsilon} = 10$ s^{-1}, were conducted by a transmission electron microscope JEOL JEM 2100 HRTEM, Tokyo, Japan, operated at a nominal voltage of 200 kV to visualize the precipitation morphology for both conditions. For this purpose, 3 mm discs were taken from the deformed zones of the hot-formed specimens and ground to 150 µm prior to electro-polishing with an electrolyte solution of 25% nitric acid + 75% methanol.

3. Results

3.1. Flow Stress Behavior at Different Temperatures and Strain Rates

The hot deformation behavior of the investigated microstructures, as-quenched and TSM, of the precipitation-hardenable aluminum alloy AA7075 at different deformation temperatures and strain rates is shown in Figure 1a–d. An increase in flow stress, represented by the peak stress σ_p, is observed for both conditions when increasing the strain rate from $\dot{\varepsilon} = 0.1$ s^{-1} to $\dot{\varepsilon} = 10$ s^{-1}, and decreasing the deformation temperatures from $T_{DT} = 350$ °C to $T_{DT} = 200$ °C. This effect of temperature and strain rate on σ_p is also visible in Figure 2. For lower deformation temperatures, the difference in the peak stress of both conditions is significantly higher than for higher temperatures. This can be seen by the arrows drawn in Figure 1a,d. However, higher flow stress levels can be seen in all cases for the as-quenched condition compared to the TSM, Figure 1a–d. However, the obtained flow curves ($\sigma_{true} - \varepsilon_{true\ plastic\ strain}$) exhibit for both conditions a distinct increase in flow stress at the beginning of the deformation before mainly a trend of continuously decreasing values is observed, indicating the occurrence of dynamic recrystallization. The occurrence of dynamic recrystallization and the associated decrease in flow stress is also shown for different aluminum alloys in other studies [10,34,35]. For the as-quenched condition at the deformation temperature of $T_{DT} = 200$ °C and the strain rate of $\dot{\varepsilon} = 0.1$ s^{-1}, the flow stress seems to stabilize earlier than the other conditions to a steady state remaining almost unchanged at the same level.

3.2. Strain-Hardening Behavior at Different Temperatures and Strain Rates

In addition to the measured hot deformation curves, the strain-hardening behavior of the as-quenched and TSM condition is plotted as the strain-hardening rate in dependence on true plastic strain $\varepsilon_{plastic\ true}$ in Figure 3a–f at deformation temperatures ranging from $T_{DT} = 200$ °C to $T_{DT} = 350$ °C and at strain rates of $\dot{\varepsilon} = 0.1$ s^{-1}, and $\dot{\varepsilon} = 10$ s^{-1}. To obtain the value of the strain-hardening rate θ, the following equation is used:

$$\theta|_i = \left.\frac{d\sigma}{d\varepsilon}\right|_i = \frac{\sigma|_{i+1} - \sigma|_{i-1}}{\varepsilon|_{i+1} - \varepsilon|_{i-1}} \quad (1)$$

The hardening curves are then divided into four stages, which are discerned by characteristic discontinuities within the course of plastic deformation, induced by microstructural phenomena at elevated temperatures. The differentiation is carried out by the changes in the slope and the inflection point of the strain-hardening curve, according to McQueen et al. [2,13]. In the first stage (Stage I), a high strain-hardening rate is obtained for both conditions at the initial stage of plastic deformation, which decreases with increasing flow stress with a high negative gradient. The hardening rate in this region is caused by a distinct dislocation multiplication and subgrain formation. Moreover, the negative gradient of the hardening rate–true stress ($\theta - \sigma_{true}$) curve in this stage is higher at the deformation temperature of $T_{DT} = 200$ °C for the as-quenched condition compared to the TSM, see Figure 3. With the increasing flow stress in the second stage (Stage II), the decrease in strain-hardening rate θ is accelerated to the first inflection point, which reflects the onset of dynamic recrystallization. With the decreasing deformation temperature and increasing strain rate, the onset of dynamic recrystallization occurs for both conditions at higher levels of the strain-hardening rate θ, as can be seen in Figure 3a–f. Before attaining the peak stress σ_p, the increased work hardening leads to a critical microstructure condition, where next to

the continuous nucleation of new grains and growth of new high-angle grain boundaries, the dislocation density increases significantly. For this reason, the measured flow stress for the as-quenched and TSM conditions increases from σ_c to σ_p, Figure 5a, but the hardening rate continuously decreases, see Figure 3 (Stage II). In stage III, the strain-hardening rate θ converges to zero at the maximum flow stress σ_p with nearly no further increase in the flow stress due to the rising fraction of dynamic recrystallization.

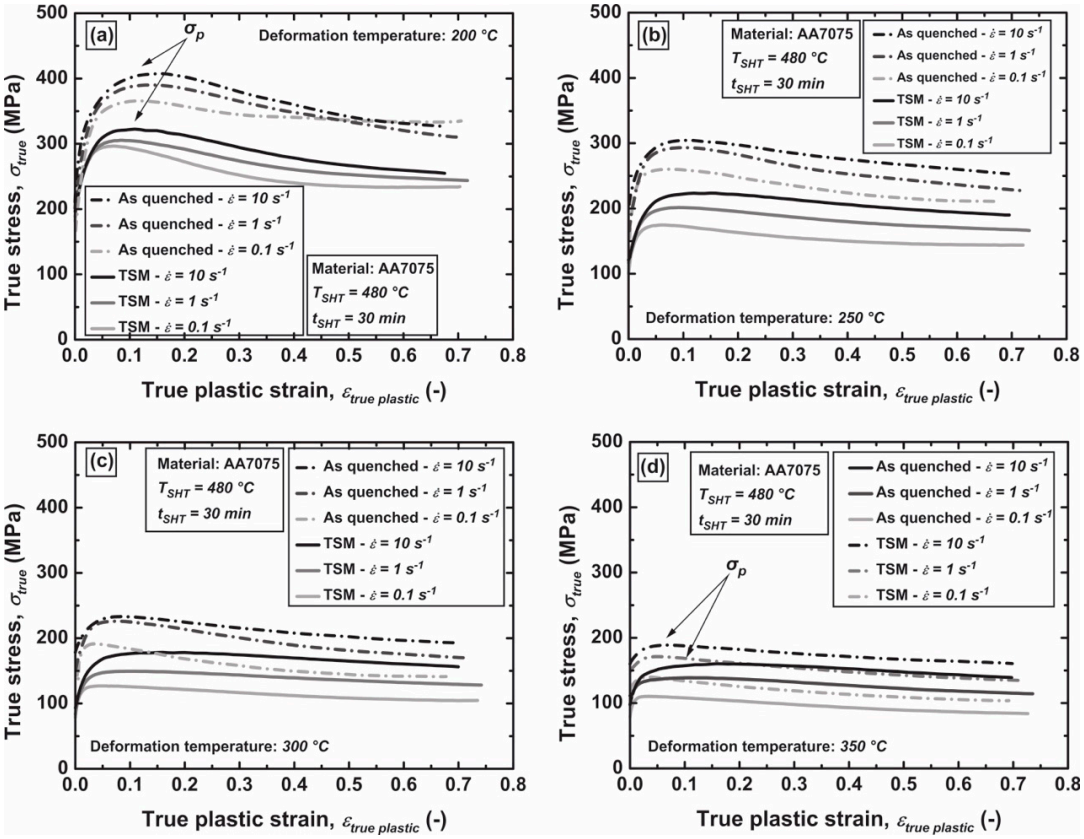

Figure 1. Hot deformation behavior of the precipitation-hardenable aluminum alloy AA7075 at different deformation temperatures of (**a**) $T_{DT} = 200$ °C, (**b**) $T_{DT} = 250$ °C, (**c**) $T_{DT} = 300$ °C and (**d**) $T_{DT} = 350$ °C and strain rates ranging from $\dot{\varepsilon} = 0.1$ s^{-1} to $\dot{\varepsilon} = 10$ s^{-1}. The solid lines show the true stress–plastic strain curves of TSM condition and the dashed lines the hot deformation curves of the as-quenched condition.

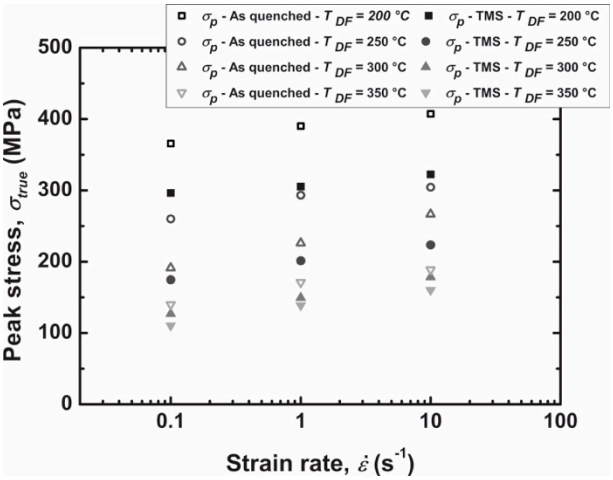

Figure 2. Measured peak stress σ_p of as-quenched and TSM conditions.

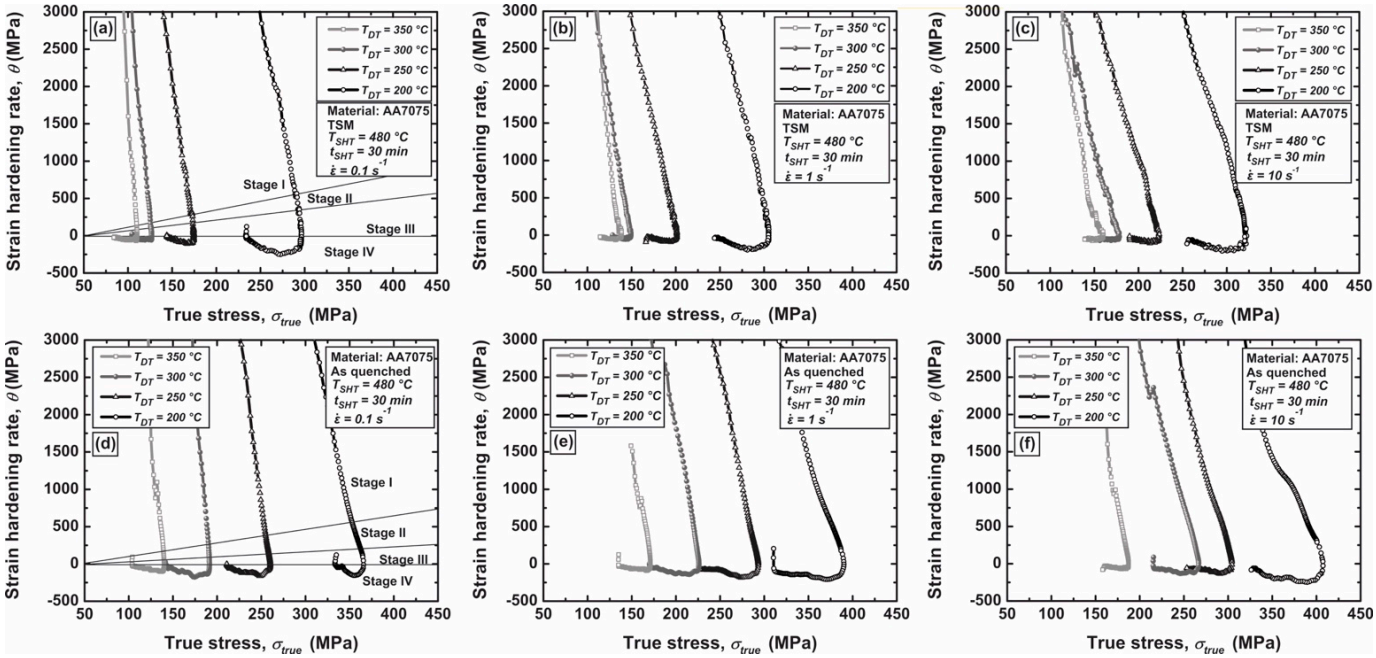

Figure 3. Strain-hardening behavior of the investigated precipitation-hardenable aluminum alloy AA7075 at deformation temperatures ranging from $T_{DT} = 200$ °C to $T_{DT} = 350$ °C and strain rates from $\dot{\varepsilon} = 0.1$ s^{-1} to $\dot{\varepsilon} = 10$ s^{-1} for (**a**–**c**) TSM and (**d**–**f**) for as-quenched and conditions.

For the as-quenched condition and at the same deformation temperature and strain rate the true stress σ_{true} reaches higher values at $\theta = 0$ MPa compared to the TSM. In the last stage (Stage IV), a transition to a negative strain-hardening rate takes place due to the dominance of softening processes and the first cycle of dynamic recrystallization becomes complete reaching an equilibrium between ongoing hardening and softening. In this stage, the level of measured strain-hardening rate values of the TSM is higher (the resulted curves of the TSM are above those of the as-quenched) compared to those of the as-quenched condition, except for the deformation temperature of $T_{DT} = 200$ °C, which will be explained in detail in the next paragraph. However, taking all strain-hardening curves into account, it becomes obvious that with increasing strain rate and decreasing deformation temperatures, all hardening curves shift to higher flow stresses, see Figure 3a–f.

For a better comparison and representation of the obtained strain-hardening behavior of the as-quenched and TSM conditions during hot deformation, strain-hardening ($\theta - \varepsilon_{plastic\ true}$) curves are further considered in this study, as can be seen in Figure 4. Note that the trend of the strain-hardening behavior of this deformation temperature is different compared to higher deformation temperatures, as described above, since the strain-hardening curves of the as-quenched condition are higher compared to those of the TSM condition. This figure illustrates the strain-hardening rate as the function of true plastic strain at the deformation temperature of $T_{DT} = 200$ °C for both conditions at the strain rate of $\dot{\varepsilon} = 0.1$ s^{-1}. In this regard, at the same level as the true plastic strain of $\varepsilon_{plastic\ true} = 0.2$ (Stage IV) and strain rate of $\dot{\varepsilon} = 0.1$ s^{-1}, the resulting strain-hardening rate θ values from the course of hardening rate–stress ($\theta - \sigma_{true}$) curves for the TSM condition is $\theta = -249$ MPa and for the as-quenched condition $\theta = -155$ MPa. Thus, it is clear from this figure that the hardening rate of the as-quenched condition is higher compared to those of the TSM condition only in the case of the deformation temperature of $T_{DT} = 200$ °C, leading to less softening.

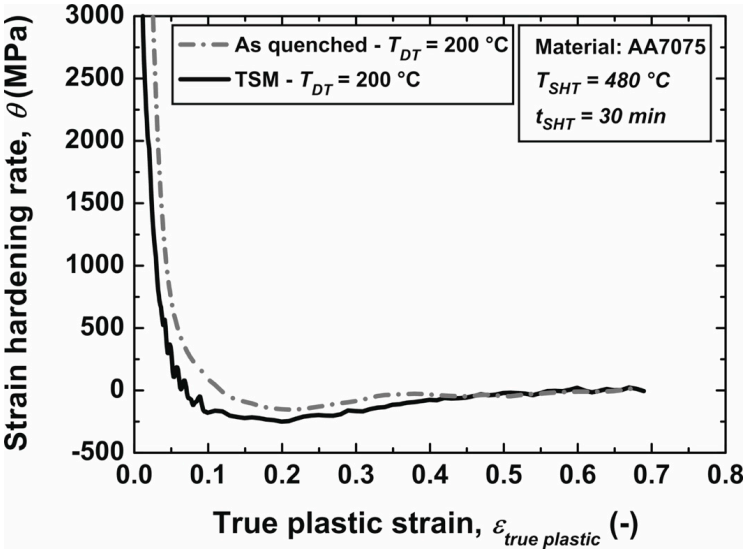

Figure 4. Strain-hardening rate of as-quenched and TSM conditions in function of true plastic strain $\varepsilon_{plastic\ true}$ at the deformation temperature of $T_{DT} = 200$ °C and strain rate of $\dot{\varepsilon} = 0.1\ s^{-1}$.

However, for the TSM condition, the measured strain-hardening values are higher for the onset of dynamic recrystallization compared to the as-quenched condition. These phenomena can be seen in Figure 5c for the selected deformation temperature of $T_{DT} = 250$ °C and the strain rate of $\dot{\varepsilon} = 0.1\ s^{-1}$ for both microstructural conditions. The onset of dynamic recrystallization during hot deformation leads to an inflection point in the measured $\theta - \sigma_{true}$ plots, which is identified in this study by fitting the third-order polynomial from zero up to the peak stress σ_p, by the mathematical approximation proposed in [36,37]. Consequently, this can be described as follows:

$$\theta = A\sigma_{true}^3 + B\sigma_{true}^2 + C\sigma_{true} + D \tag{2}$$

where A, B and D are the constants for a given hot deformation condition. From Figure 5b it is obvious that the measured experimental $\theta - \sigma_{true}$ curves and the fitted data coincide, and no significant differences appear. The second derivation of this equation with respect to true stress σ_{true} can be expressed as:

$$\frac{d^2\theta}{d\sigma_{true}^2} = 6A\sigma_{true} + 2B \tag{3}$$

Consequently, the initiation of dynamic recrystallization, and thus, the critical stress σ_c is obtained by the minimum of Equation (3), where the second derivative equals zero:

$$6A\sigma_{true} + 2B = 0 \rightarrow \ \sigma_c = \frac{2B}{6A} \tag{4}$$

Figure 5c shows the obtained σ_c for the selected deformation temperature of $T_{DT} = 250$ °C and at the strain rate of $\dot{\varepsilon} = 0.1\ s^{-1}$.

Figure 6 summarizes all hardening parameters, σ_c and θ for the as-quenched and TSM microstructures at deformation temperatures ranging from $T_{DT} = 200$ °C to $T_{DT} = 350$ °C and strain rates from $\dot{\varepsilon} = 0.1\ s^{-1}$ to $\dot{\varepsilon} = 10\ s^{-1}$. Note that the interpolation approach thin plate spline interpolation is carried for the calculated parameters.

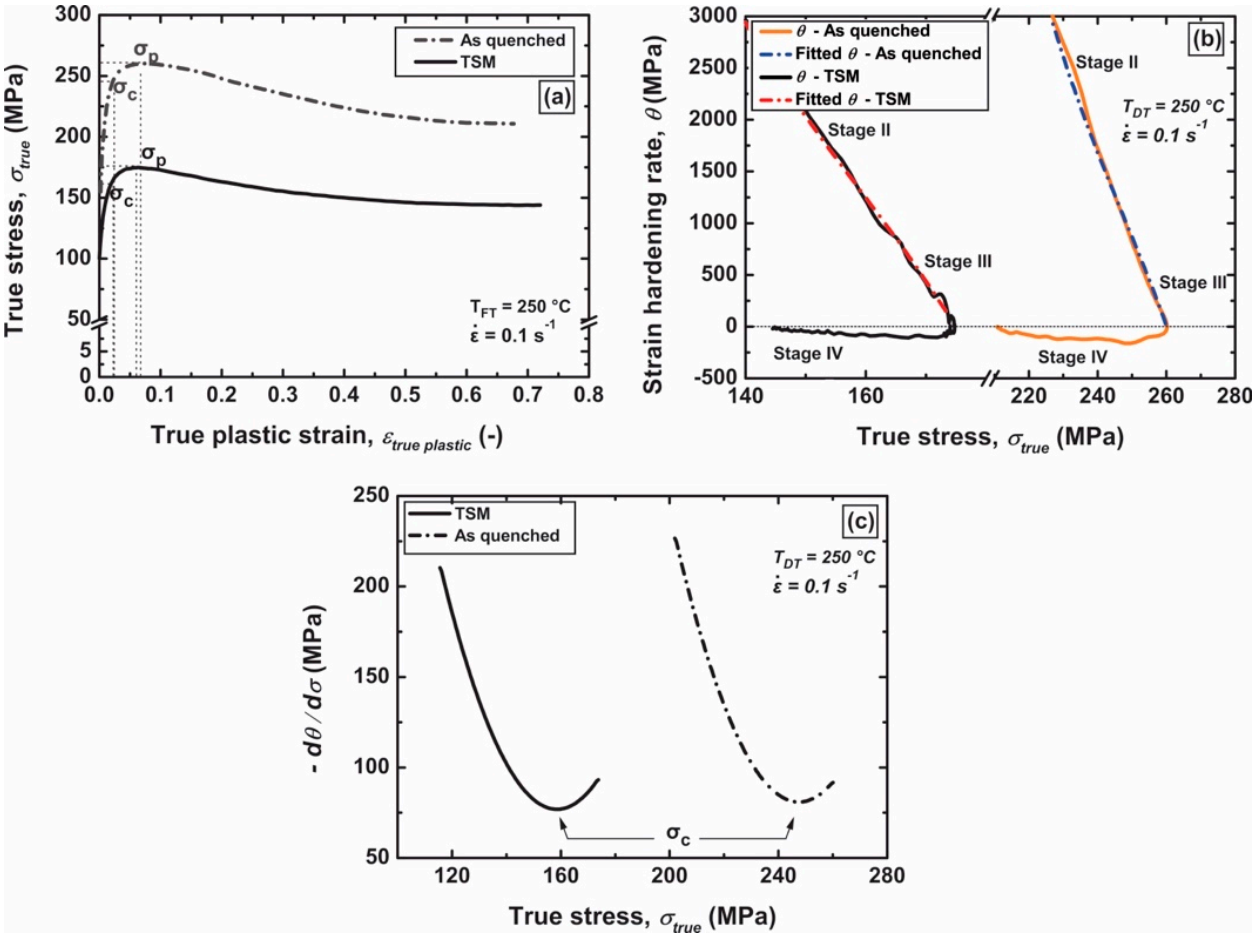

Figure 5. (**a**) Selected hot deformation behavior of the as-quenched and TSM microstructures at deformation temperature of $T_{DT} = 250$ °C and strain rate of $\dot{\varepsilon} = 0.1$ s^{-1} to determine the critical stress. (**b**) Measured experimental and fitted strain-hardening rate θ and (**c**) derivation of the $\theta - \sigma_{true}$ plot with respect to true stress σ_{true}, to represent the critical stress σ_c at the minimum of $d\theta/d\sigma_{true}$.

3.3. Microstructure Investigation

In Figure 7a–d, the hot-formed microstructures of the as-quenched and TSM condition are shown for the strain rates of $\dot{\varepsilon} = 0.1$ s^{-1} and $\dot{\varepsilon} = 10$ s^{-1} and the deformation temperature of $T_{DT} = 200$ °C. In the case of the TSM condition, coarse and non-uniformly distributed precipitates are visible for both strain rates. The as-quenched microstructure exhibits, in contrast, a lower number of precipitates and second phases within the formed grains. However, the amount and the size of the very fine precipitates of this microstructure are slightly higher at a low strain rate, implying the occurrence of dynamic precipitation. This thermo-mechanically activated phenomenon is enabled by a sufficient nucleation time at a low strain rate of $\dot{\varepsilon} = 0.1$ s^{-1} at $T_{DT} = 200$ °C as well as by a high number of nucleation sites for very fine clusters and precipitates created by dislocation multiplication, Figure 7d. The observation of the very fine cluster requires electron microscopy techniques with a near-atomic resolution, which is not the focus of the present study. However, based on the obtained mechanical properties, the presence of very fine particles can be assumed for the as-quenched condition. Moreover, the TEM-micrograph for the TSM condition reveals a higher dislocation density with narrow and likely bounded structure (BDS) within the formed grains. Based on the dislocation slip and climb, this dislocation multilateralization for the TSM-formed microstructure is mainly the result of dynamic recovery, see Figure 7a,b.

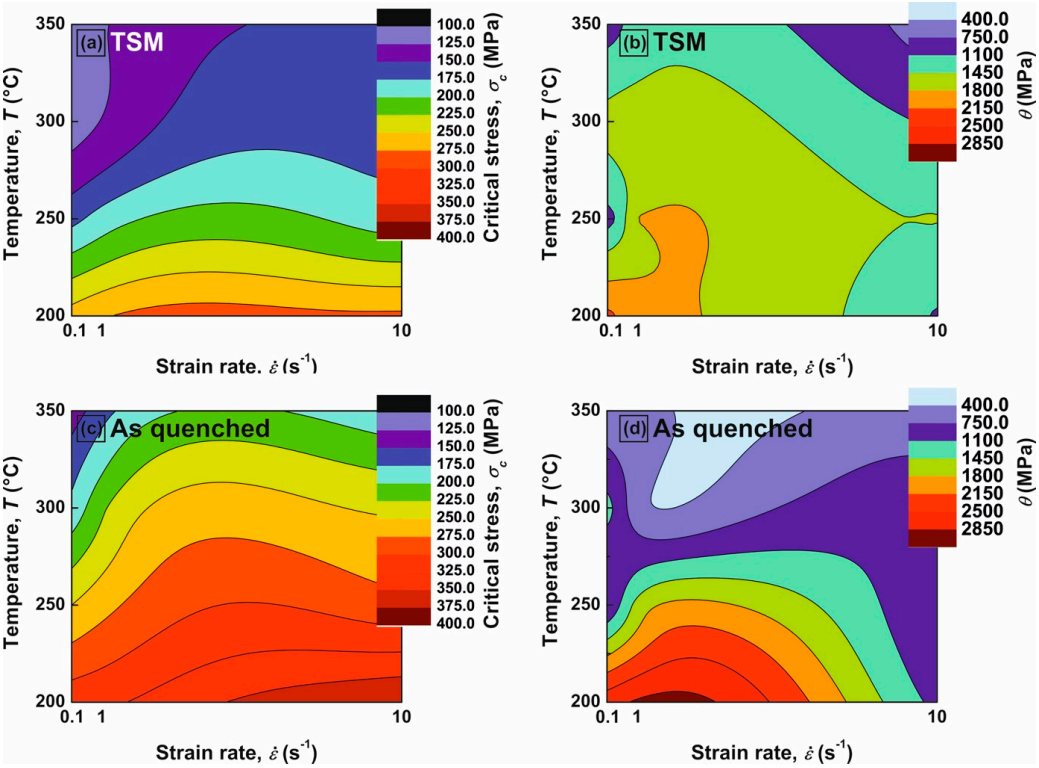

Figure 6. Strain-hardening parameter of the investigated precipitation-hardenable aluminum alloy AA7075 at deformation temperatures ranging from $T_{DT} = 200$ °C to $T_{DT} = 350$ °C and strain rates from $\dot{\varepsilon} = 0.1$ s^{-1} to $\dot{\varepsilon} = 10$ s^{-1} for (**a**,**b**) TSM and (**c**,**d**) for as-quenched conditions.

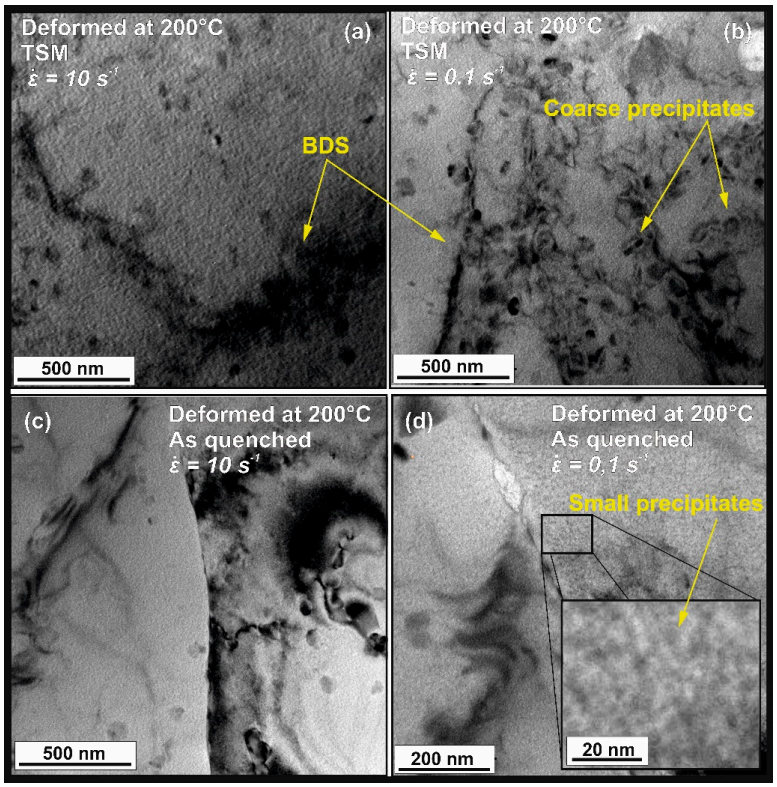

Figure 7. TEM- micrograph of TSM condition deformed at $T_{DT} = 200$ °C and strain rates of (**a**) $\dot{\varepsilon} = 10$ s^{-1} and (**b**) strain rates of $\dot{\varepsilon} = 0.1$ s^{-1}. TEM- micrograph of as-quench condition deformed at $T_{DT} = 200$ °C and strain rates of (**c**) $\dot{\varepsilon} = 10$ s^{-1} and (**d**) strain rates of $\dot{\varepsilon} = 0.1$ s^{-1}.

Figure 8 shows the deformed microstructure of the as-quenched condition at the deformation temperature of $T_{DT} = 200$ °C and strain rate of $\dot{\varepsilon} = 0.1$ s^{-1} for better visualization of the precipitate distribution. From this figure, fine and homogenously distributed precipitates can be seen. Moreover, coarse precipitates are also observed for this condition due to the used deformation temperature. Hence, this condition exhibits a mixed microstructure consisting of predominantly fine and few coarse precipitates.

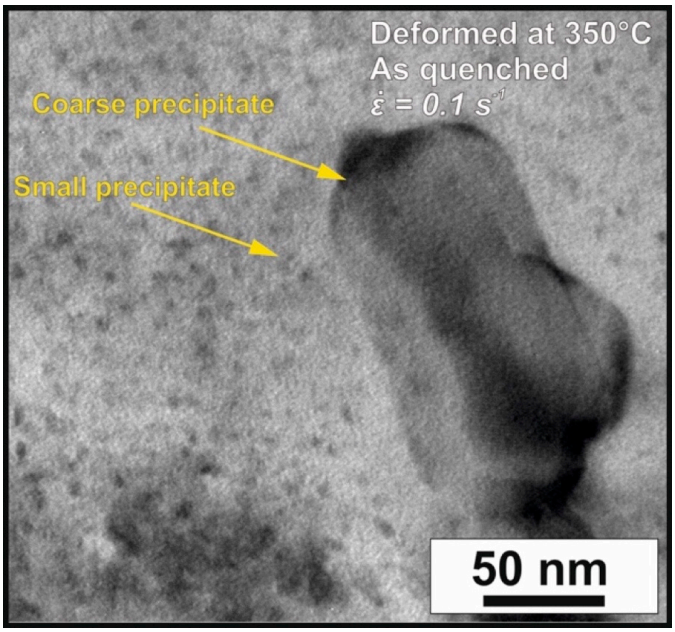

Figure 8. TEM micrograph of the formed microstructure at the deformation temperature of $T_{DT} = 200$ °C and strain rate of $\dot{\varepsilon} = 0.1$ s^{-1} of the as-quenched condition.

Figure 9a,b show the microstructure of both conditions at the deformation temperature of $T_{DT} = 350$ °C and strain rate of $\dot{\varepsilon} = 10$ s^{-1}. For the TSM microstructure, lath-shaped and coarse particles can be seen within the recrystallized grains. These particles are referred to in the literature at 350 °C to equilibrium η-phase for the precipitation-hardenable aluminum alloy AA7075 [38–40]. Due to the high thermal energy at the aging temperature prior to hot deformation, GP-zones and η'-phase can transform to incoherent η-phases, which hardly contribute to the material strength. In the case of the as-quenched microstructure, a reduced number of η-phases and coarse precipitates are detected, instead of this a high quantity of fine precipitates after hot deformation could be found, showing the dependence of precipitation formation to the applied heat treatment strategy. In terms of the nature of precipitation-hardening mechanisms expressed in the following equation [41–43]:

$$\Delta\sigma_p = c f^{1/2} r^{-1} \tag{5}$$

a decrease in precipitates radius r means high material strength and finally higher flow stresses during plastic deformation, whereas c is an alloy constant and f a volume fraction of precipitates.

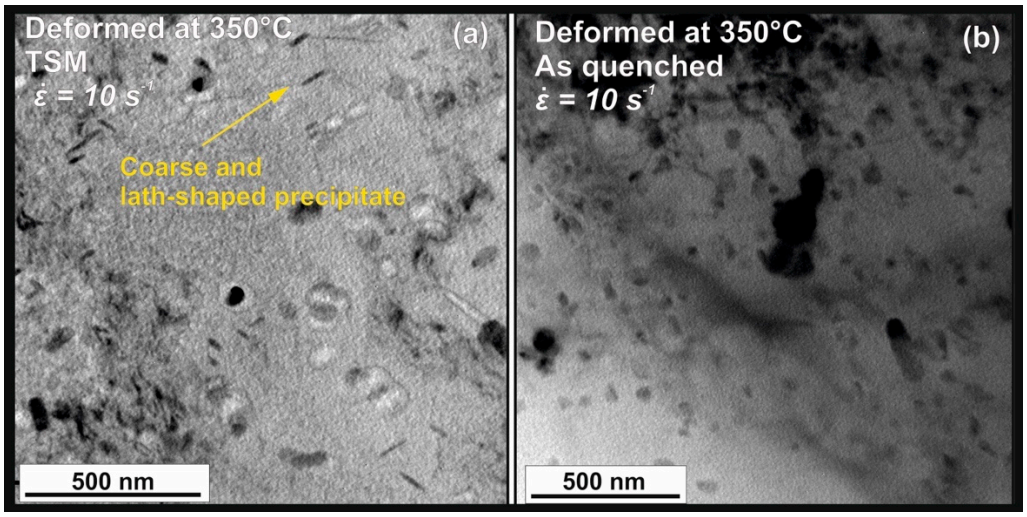

Figure 9. TEM micrograph of the formed microstructure at the deformation temperature of $T_{DT} = 350$ °C and strain rates of $\dot{\varepsilon} = 10$ s^{-1} for (**a**) TSM condition and (**b**) as-quenched condition.

4. Discussion

The above-presented results show that, in general, the obtained flow stress increases when decreasing the deformation temperature and increasing the strain rate. This behavior is an expected result of the thermally activated lattice vibration promoting atom displacements and dislocation movements. Low thermal energy levels at decreased deformation temperatures increase the required mechanical energy to activate and maintain dislocation movement significantly. Moreover, the reduction of thermal energy leads to reduced activation of cross-slip processes of screw dislocations and hinders, therefore, the overcoming of dislocation movement obstacles [43,44]. The influence of the strain rate can be explained by the time dependency of thermally activated mechanisms and the influence on the probability of slip processes per unit of time. With increasing strain rate, the probability of slip processes per unit of time increases, reducing the remaining time for thermally activated softening processes such as dynamic recovery and recrystallization.

On the other hand, it is observed that the as-quenched condition obtains, in all cases, higher flow stress levels than the TSM condition. This behavior results from the dynamic precipitation of a metastable supersaturated microstructure during hot deformation leading to precipitation hardening. The nucleated fine particles increase the required stress for moving dislocations to overcome the newly formed obstacles. For the TSM condition, in contrast, the coarse equilibrium precipitates, obtained during the artificial aging treatment prior to hot deformation, hardly contribute to a flow stress increase.

The strain-hardening rate of both conditions revealed characteristic phenomena, such as the onset of dynamic recrystallization appearing at lower critical stresses when increasing the deformation temperature. At the beginning of deformation and at low deformation temperatures of $T_{DT} = 200$ °C, the obtained strain-hardening rate depends for both conditions mainly on the dislocation–dislocation interactions, due to the low amount of precipitates, see Figure 3. Moreover, for the as-quenched condition, the possible nucleation of very fine particles along the grain boundaries hinders the motion of low- as well as high-angle grain boundaries leading to a local accumulation of dislocations and hindering their elimination. With an increasing deformation temperature and plastic deformation level, the induced dynamic precipitation prevails and moving dislocations predominantly interact with very fine distributed particles. Due to the high number of generated dislocations in the initial deformation stage of the as-quenched condition, dynamic recrystallization occurs at lower critical strains compared to the TSM microstructure. However, it should be noted that both mechanisms, dynamic precipitation and dislocation multiplication, are simultaneously responsible for the obtained higher flow stress of the as-quenched condition. In the case of the TSM condition, the measured hardening rate θ in the later stages of deformation

is higher, as is the noticeably increased particle size and, therefore, the large dislocation mean free path reduces the dislocation particle interactions significantly [39,45]. This phenomenon is explained by the fact that strain hardening is proportional to the ratio of the volume fraction to the size of particles or to the interparticle spacing. The TEM observations confirm the presence of very coarse particles for the TSM condition and the formation of cell walls by dislocation polygonization.

5. Conclusions

The influence of different microstructural conditions on the hot deformation behavior of the precipitation-hardenable aluminum alloy AA7075 during compression tests is studied in the present work. Summing up the results of the present work on the influence of different microstructural conditions on the hot deformation behavior of the precipitation-hardenable aluminum alloy AA7075, the following conclusions are drawn:

- Microstructural condition, deformation temperature and strain rate have a significant effect on the prevailing hardening and softening mechanisms of the precipitation-hardenable aluminum alloy AA7075, which determines the resulting hot deformation behavior. In the case of the deformation temperature of 200 °C and strain rate of 10 $s^{-1,}$ a 110 MPa higher peak stress is obtained for the as-quenched microstructure compared to the TSM.
- A higher flow stress level was obtained for the as-quenched condition compared to the TSM in all cases. This behavior can be linked to the dynamic precipitation during hot deformation for the metastable as-quenched condition, leading to higher required stress for moving dislocations to overcome the nucleated fine particles. For the TSM condition, in contrast, coarse and equilibrium precipitates are obtained during the artificial treatment prior to hot deformation, which hardly contributes to the flow stress increase.
- The choice of deformation temperature and strain rate determines the onset of softening mechanisms leading to correspondingly high or low levels of flow stress.
- The microstructural condition prior to the hot deformation influences the hardening mechanisms. The hardening of a stable condition of precipitations is mainly driven by dislocation–dislocation interactions, whilst the metastable supersaturated solid solution of the as-quenched condition experiences a change from strain hardening to dislocation–particle interactions due to the activation of dynamic precipitation.

Author Contributions: Conceptualization, E.S. and J.A.N.; methodology, E.S. and J.A.N.; hot deformation experiment, J.A.N. and A.Q.; microstructure investigation, E.S.; writing—original draft preparation, E.S.; writing—review and editing, U.W., J.A.N., A.Q. and E.S.; visualization, E.S., J.A.N. and A.Q.; supervision, U.W. and K.S.; project administration, K.S. All authors have read and agreed to the published version of the manuscript.

Funding: The authors would like to thank the Hessen State Ministry for Higher Education, Research and the Arts—Initiative for the Development of Scientific and Economic Excellence (LOEWE), for the financial support of the special research project "ALLEGRO".

Data Availability Statement: Not applicable.

Acknowledgments: The authors would like to thank Stefan Seidel for sample preparation.

Conflicts of Interest: The authors declare no conflict of interest. The funders had no role in the design of the study; in the collection, analyses, or interpretation of data; in the writing of the manuscript; or in the decision to publish the results.

References

1. Steinhoff, K.; Weidig, U.; Saba, N. Investigation of plastic forming under the influence of locally and temporally variable temperature and stress states. In *Functionally Graded Materials in Industrial Mass Production*; Steinhoff, K., Maier, H.J., Biermann, D., Eds.; Verlag Wissenschaftliche Scripten: Auerbach/Vogtland, Germany, 2009; pp. 35–52.
2. McQueen, H.J.; Imbert, C.A.C. Dynamic recrystallization: Plasticity enhancing structural development. *J. Alloys Compod.* **2004**, *378*, 35–43. [CrossRef]
3. Steinhoff, K.; Maikranz-Valentin, M.; Saba, N.; Weidig, U. Position and time dependent thermo-mechanical treatment of sheet steel for light weight structures. In Proceedings of the Herstellung und Weiterverarbeitung von Flachprodukten, TU Bergakad, Freiberg, Germany, 25–27 March 2009; pp. 130–144.
4. Raabe, D. Cellular Automata in Materials Science with Particular Reference to Recrystallization Simulation. *Annu. Rev. Mater. Res.* **2003**, *32*, 53–76. [CrossRef]
5. Steinhoff, K.; Weidig, U.; Bergmann, K.; Elsner, A. Verfahren zur Herstellung Eines zum Formhärten Geeigneten Blechhalbzeugs. German Patent DE102006032617B4, 12 July 2006.
6. Maikranz-Valentin, M.; Weidig, U.; Schoof, U.; Becker, H.; Steinhoff, K. Components with Optimised Properties due to Advanced Thermo-mechanical Process Strategies in Hot Sheet Metal Forming. *Steel Res. Int.* **2008**, *79*, 92–97. [CrossRef]
7. Gottstein, G. *Materialwissenschaft und Werkstofftechnik*; Springer-Lehrbuch; Springer: Berlin/Heidelberg, Germany, 2015; ISBN 978-3-642-36602-4.
8. Hornbogen, E.; Warlimont, H. Strukturen fester phasen. In *Metallkunde*; Springer: Berlin/Heidelberg, Germany, 2001; pp. 24–42.
9. Zhang, J.; Yi, Y.; Huang, S.; Mao, X.; He, H.; Tang, J.; Guo, W.; Dong, F. Dynamic recrystallization mechanisms of 2195 aluminum alloy during medium/high temperature compression deformation. *Mater. Sci. Eng. A* **2021**, *804*, 140650. [CrossRef]
10. McQueen, H.J.; Hockett, J.E. Microstructures of aluminum compressed at various rates and temperatures. *Metall. Trans.* **1970**, *1*, 2997–3004. [CrossRef]
11. Raabe, D. Mesoscale simulation of recrystallization textures and microstructures. *Adv. Eng. Mater.* **2001**, *3*, 745–752. [CrossRef]
12. Li, Y.; He, C.; Wei, J.; Zhang, Z.; Tian, N.; Qin, G.; Zhao, X. Effect of Post-Fabricated Aging on Microstructure and Mechanical Properties in Underwater Friction Stir Additive Manufacturing of Al–Zn–Mg–Cu Alloy. *Materials* **2022**, *15*, 3368. [CrossRef] [PubMed]
13. McQueen, H.J.; Spigarelli, S.; Kassner, M.E.; Evangelista, E. *Hot Deformation and Processing of Aluminum Alloys*; 1.; CRC Press: Boca Raton, FL, USA, 2011; ISBN 9781420017687.
14. Sajadifar, S.V.; Scharifi, E.; Wegener, T.; Krochmal, M.; Lotz, S.; Steinhoff, K.; Niendorf, T. On the low-cycle fatigue behavior of thermo-mechanically processed high-strength aluminum alloys. *Int. J. Fatigue* **2022**, *156*, 106676. [CrossRef]
15. Sajadifar, S.V.; Scharifi, E.; Weidig, U.; Steinhoff, K.; Niendorf, T. Performance of thermo-mechanically processed AA7075 alloy at elevated temperatures—From microstructure to mechanical properties. *Metals* **2020**, *10*, 884. [CrossRef]
16. Shojaei, K.; Sajadifar, S.V.; Yapici, G.G. On the mechanical behavior of cold deformed aluminum 7075 alloy at elevated temperatures. *Mater. Sci. Eng. A* **2016**, *670*, 81–89. [CrossRef]
17. Mianroodi, J.R.; Rezaei, S.; Siboni, N.H.; Xu, B.X.; Raabe, D. Lossless multi-scale constitutive elastic relations with artificial intelligence. *NPJ Comput. Mater.* **2022**, *8*, 67. [CrossRef]
18. Sakai, T.; Takahashi, C. Flow Softening of 7075 Aluminum Alloy under Hot Compression. *Mater. Trans. JIM* **1991**, *32*, 375–382. [CrossRef]
19. Völkers, S.; Scharifi, E.; Sajjadifar, S.V.; Böhm, S.; Weidig, U.; Niendorf, T. On the influence of in situ sound wave superposition on the microstructure of laser welded 7000 aluminum alloys. *J. Adv. Join. Process.* **2020**, *1*, 100013. [CrossRef]
20. Roven, H.J.; Liu, M.; Werenskiold, J.C. Dynamic precipitation during severe plastic deformation of an Al–Mg–Si aluminium alloy. *Mater. Sci. Eng. A* **2008**, *483–484*, 54–58. [CrossRef]
21. Zhang, Y.; Jin, S.; Trimby, P.W.; Liao, X.; Murashkin, M.Y.; Valiev, R.Z.; Liu, J.; Cairney, J.M.; Ringer, S.P.; Sha, G. Dynamic precipitation, segregation and strengthening of an Al-Zn-Mg-Cu alloy (AA7075) processed by high-pressure torsion. *Acta Mater.* **2019**, *162*, 19–32. [CrossRef]
22. Deschamps, A.; Fribourg, G.; Bréchet, Y.; Chemin, J.L.; Hutchinson, C.R. In situ evaluation of dynamic precipitation during plastic straining of an Al-Zn-Mg-Cu alloy. *Acta Mater.* **2012**, *60*, 1905–1916. [CrossRef]
23. Couturier, L.; Deschamps, A.; De Geuser, F.; Fazeli, F.; Poole, W.J. An investigation of the strain dependence of dynamic precipitation in an Al-Zn-Mg-Cu alloy. *Scr. Mater.* **2017**, *136*, 120–123. [CrossRef]
24. Chen, C.; Chen, J.; Yan, H.; Su, B.; Song, M.; Zhu, S. Dynamic precipitation, microstructure and mechanical properties of Mg-5Zn-1Mn alloy sheets prepared by high strain-rate rolling. *Mater. Des.* **2016**, *100*, 58–66. [CrossRef]
25. Cubides, Y.; Zhao, D.; Nash, L.; Yadav, D.; Xie, K.; Karaman, I.; Castaneda, H. Effects of dynamic recrystallization and strain-induced dynamic precipitation on the corrosion behavior of partially recrystallized Mg–9Al–1Zn alloys. *J. Magnes. Alloys* **2020**, *8*, 1016–1037. [CrossRef]
26. Kabir, A.S.H.; Su, J.; Jung, I.H.; Yue, S. Study of Dynamic Precipitation during Hot Deformation of Mg-Al-Sn Alloys. *Mater. Sci. Forum* **2013**, *765*, 461–465.
27. Heider, B.; Scharifi, E.; Engler, T.; Oechsner, M.; Steinhoff, K. Influence of heated forming tools on corrosion behavior of high strength aluminum alloys. *Materwiss. Werksttech.* **2020**, *52*, mawe.202000125. [CrossRef]

28. Scharifi, E.; Sajadifar, S.V.; Moeini, G.; Weidig, U.; Böhm, S.; Niendorf, T.; Steinhoff, K. Dynamic Tensile Deformation of High Strength Aluminum Alloys Processed Following Novel Thermomechanical Treatment Strategies. *Adv. Eng. Mater.* **2020**, *22*, 2000193. [CrossRef]
29. Scharifi, E.; Shoshmina, D.; Biegler, S.; Weidig, U.; Steinhoff, K. Influence of hot deformation on the precipitation hardening of high-strength aluminum aa7075 during thermo-mechanical processing. *Metals* **2021**, *11*, 681. [CrossRef]
30. Scharifi, E.; Knoth, R.; Weidig, U. Thermo-mechanical forming procedure of high strength Aluminum sheet with improved mechanical properties and process efficiency. *Procedia Manuf.* **2019**, *29*, 481–489. [CrossRef]
31. Scharifi, E.; Erbskorn, F.; Ademaj, A.; Kavaklioglu, Z.B.; Weidig, U.; Steinhoff, K. Potentialities of process cycle time reductions at hot stamping of aluminum alloys. In Proceedings of the 7th International Conference Hot Sheet Metal Forming on High Performance Steel, Luleå, Sweden, 2–5 June 2019; Volume 6082, pp. 237–245.
32. *Richtlinie zur Aufnahme von Fließkurven*; German Cold Forming Group, German Forging Association: Hagen, Germany, 2008. (In German)
33. Kopp, R.; Luce, R.; Leisten, B.; Wolske, M.; Tschirnich, M.; Rehrmann, T.; Volles, R. Flow stress measuring by use of cylindrical compression test and special application to metal forming processes. *Steel Res.* **2001**, *72*, 394–401. [CrossRef]
34. Li, K.; Pan, Q.; Li, R.; Liu, S.; Huang, Z.; He, X. Constitutive Modeling of the Hot Deformation Behavior in 6082 Aluminum Alloy. *J. Mater. Eng. Perform.* **2019**, *28*, 981–994. [CrossRef]
35. Jonas, J.J.; Quelennec, X.; Jiang, L.; Martin, É. The Avrami kinetics of dynamic recrystallization. *Acta Mater.* **2009**, *57*, 2748–2756. [CrossRef]
36. Najafizadeh, A.; Jonas, J.J. Predicting the critical stress for initiation of dynamic recrystallization. *ISIJ Int.* **2006**, *46*, 1679–1684. [CrossRef]
37. Poliak, E.I.; Jonas, J.J. Initiation of Dynamic Recrystallization in Constant Strain Rate Hot Deformation. *ISIJ Int.* **2003**, *43*, 684–691. [CrossRef]
38. Buha, J.; Lumley, R.N.; Crosky, A.G. Secondary ageing in an aluminium alloy 7050. *Mater. Sci. Eng. A* **2008**, *492*, 1–10. [CrossRef]
39. Scharifi, E.; Savaci, U.; Kavaklioglu, Z.B.; Weidig, U.; Turan, S.; Steinhoff, K. Effect of thermo-mechanical processing on quench-induced precipitates morphology and mechanical properties in high strength AA7075 aluminum alloy. *Mater. Charact.* **2021**, *174*, 111026. [CrossRef]
40. Huo, W.; Hou, L.; Zhang, Y.; Zhang, J. Warm formability and post-forming microstructure/property of high-strength AA 7075-T6 Al alloy. *Mater. Sci. Eng. A* **2016**, *675*, 44–54. [CrossRef]
41. Hornbogen, E. Hundred years of precipitation hardening. *J. Light Met.* **2001**, *1*, 127–132. [CrossRef]
42. Hornbogen, E.; Starke, E.A. Overview no. 102 theory assisted design of high strength low alloy aluminum. *Acta Metall. Mater.* **1993**, *41*, 1–16. [CrossRef]
43. Jägle, E.A.; Sheng, Z.; Wu, L.; Lu, L.; Risse, J.; Weisheit, A.; Raabe, D. Precipitation Reactions in Age-Hardenable Alloys During Laser Additive Manufacturing. *Jom* **2016**, *68*, 943–949. [CrossRef]
44. Hull, D.; Bacon, D.J. *Introduction to Dislocations*; Butterworth-Heinemann: Oxford, UK, 2011; ISBN 9780080966724.
45. Strohmann, T.; Breitbarth, E.; Besel, M.; Zaunschirm, S.; Witulski, T.; Requena, G. Damage Mechanisms and Anisotropy of an AA7010-T7452 Open-Die Forged Alloy: Fatigue Crack Propagation. *Materials* **2022**, *15*, 3771. [CrossRef] [PubMed]